Revamped Electrode Models for Driving Electrochemical Reactions under Alkaline Conditions

Michael T. Tang,[*,†,‡] Michal Bajdich,[*,†] and Frank Abild-Pedersen[*,†,‡]

† *SUNCAT Center for Interface Science and Catalysis, SLAC National Accelerator Laboratory, CA, 94025, USA*

‡*Corresponding Author*

E-mail: mtt013@stanford.edu; bajdich@slac.stanford.edu; abild@slac.stanford.edu

Abstract

Driving electrochemical reaction with bias in aqueous environment is an attractive approach for sustainable chemical synthesis, but understanding reaction dynamics remains a serious challenge in electrocatalysis. Computational techniques and concepts are necessary to elucidate the underpinnings of creating catalytic sites that are highly active, selective, and stable. Herein, we elucidate the intrusive role of hydroxide ions in running electrochemical reactions under alkaline conditions. Through an overhaul of the computational hydrogen electrode (CHE), we show that hydroxide ions do adsorb on many late transition metals even under negative bias. This is even so on metals like Cu and Pt, where the OH* binding energy is energetically uphill relative to H_2O (l). We provide a computational framework for modeling reaction energetics with OH^-* relative to OH^-(aq), using HER and CO_2R as examples for how to model electroreduction reactions under alkaline conditions.

Introduction

Electrochemistry is a notable technology that can leverage the growth of renewable energy sources and develop new sustainable chemical pathways that are not dependent on fossil-fuel sources[1–3]. Current mechanistic understanding of electrochemical reactions remains lacking due to the involvement of complex interfacial morphologies. Typically, electrocatalysis involves transition metal electrodes immersed in a solvent containing some dissolved electrolyte, which then an applied potential is used to polarize the overall system to form chemical products[4].

Previous works that describe the complexities of electrochemical interfaces are highly interdisciplinary[5–11]. Even before the discovery of quantum physics, the Nernst equation relates the equilibrium potentials to ionic concentrations in cell electrolytes in 1899[5]. Peter Debye and Erich Hückel laid the foundations for understanding the chemical activities of electrolytes in solution in 1923[12]. Guggenheim describes the conundrum of determining the chemical potential of charged ion species individually in 1929[13]. In 1931, Gurney provides the first attempt in modeling electrolytic current densities with the probabilistic nature of electrons in metal electrode[14]. In 1958, Hush considered the effects of potential change in the double layer at the electrode surface in effecting electron transfer activation energies, followed by Marcus providing a theory for electron transfer reactions in 1965[5,15]. Numerous attempts to apply the understanding of metal work functions to electrochemistry[16].

Computational modeling of electrochemical cells is used to rationalize experimental observations of electrochemical reactions[15,17–23]. However, due to poor resolution of what happens at the electrochemical interface, theoretical insights remain speculative. For instance, the simulation of electrochemistry within supercells will often consider the addition of a solvation layer laid over the electrode slab. Various solvation schemes are used to incorporate the effects that water molecules may have on electrochemical reactions. While solvation models have been successful in describing certain phenomena such as the thermochemical properties

of water via molecular dynamics simulation, they become much more cumbersome to use in conjunction with DFT calculations where quantum effects are needed.

Currently, there are two popular methods to simulate the energetics of electrochemical reactions. First formulated in the work of Nørskov et al. in 2004[24], the computational hydrogen electrode (CHE) is notable for its simplicity and its ability to relate back to thermochemical catalysis. The CHE model has seen success in describing electrochemical reactions under acidic conditions but needs additional "corrections" schemes when capturing the various pH-driven effects observed in electrocatalysis performed under alkaline environments. Hence, secondary approaches such as grand-canonical density functional theory (GC-DFT) have recently seen greater adoption in simulating energetics of electrochemical cells[18]. The grand-canonical approach assumes that the electron potential of *any* electrochemical system can be referenced to the energy of an electron in vacuum[16]; furthermore, we are able to maintain an electron potential within a supercell such that the *free* energetics are held at constant potential by varying the number of electrons in the system[17,25–27]. The ability to reference an "absolute" electrode potential justifies its use in simulating pH effects in water[28,29]. The main drawback of the approach is added computational cost and uncertainty in the value of the "absolute" electrode potential and potential of zero charge (PZC). The necessity of defining a quadratic energetic relation for the supercell on the voltage may also introduce problems, which we will explain in detail. Overall, both electrode models require higher computational times to simulate conditions or complexities beyond the acidic regime: pH effects, solvation effects, cation and anion effects, and electrostatic field effects[30–39].

This work aims to simplify treatment of energetics under water reduction conditions. We will justify that the thermodynamic free energetics of charged species like $1M$ aqueous hydroxide ion can be simply treated like a typical gaseous reference based on the ionization constant of water ($\mu_{OH_0^-(aq)} = \mu_{H_2O} + 0.82eV - \frac{1}{2}\mu_{H_2}$), where $0.82eV$ is realized from $0.059 * pKa_{OH-}$. This is analogous to treating $1M$ proton via the chemical potential of H_2 gas at standard con-

ditions via the CHE model ($\mu_{H_0^+(aq)} = \frac{1}{2}\mu_{H_2}$) (in this work, we have chosen to use the term chemical potential interchangeably with chemical activity). We provide cautionary examples on where the charge-centric CHE model and grand-canonical methods may fall short. With the proposed "Computational Ion-Molecule Electrode" (CIME) model, we demonstrate that a straightforward method of determining energetics of surface intermediates can be used to model alkaline hydrogen evolution (HER) on metal-decorated Pt(111) and 2-electron CO_2R (CO_2RR) on Ag(100) and Au(100). Consequentially this work shows that, specifically under water splitting conditions, there is a driving force to adsorb hydroxide ions in the $1M$ concentration on most late transition metals. This model essentially revamps the original CHE model to capture general pH related trends regarding electrochemical reduction reactions under alkaline conditions, without resorting to other expensive computational schemes. We end by suggesting new questions and research directions that spring out of this simple treatment of charged species.

Results and discussion

Water Reduction at pH 0: The CHE Way

To start, we will use the original CHE model at pH 0 to derive the chemical potential of $1M$ OH^- in aqueous solution. For proton-electron coupled step reactions, we will notate them as:

$$X^* + H^+ + e^- \rightleftharpoons XH^* \tag{1}$$

In density functional theory, it is difficult to model a solvated proton, H^+, in a computational cell[24]. Hence, the CHE model postulates alongside the *standard* hydrogen electrode (SHE), such that there exists a potential where a standard concentration of $1M$ hydronium solution is in electrochemical equilibrium with *1 bar* atmospheric pressure of $\frac{1}{2}$ H_2 gas:

$$\mu_{H+(aq)} + \mu_{e-} = \frac{1}{2}\mu_{H_2(g)} - eU_{applied} \tag{2}$$

By definition at this potential, it takes an infinitesimal amount of *applied* electrostatic work ($-eU_{applied}$ in either the SHE or RHE scale) to convert between $\frac{1}{2}$ H_2 gas and solvated hydronium in water. This is shown in **Figure 1(a)** where under highly acidic pH 0 conditions, applying a tiny amount of energy per charge in the form of an applied potential using a platinized electrode enables fast conversion of H^+ into H_2 gas. The application of the CHE model as it is shown in Equation 2 has been largely successful in describing acidic hydrogen evolution and oxygen reduction and evolution when it was introduced in 1997 and 2004[24].

If we want to describe water splitting *at pH 0*, then we should expect to apply a greater amount of electrostatic work to split water compared to hydronium. Experimentally,[40–42] water is observed to self-ionize into hydronium and hydroxide ions:

$$H_2O + H_2O \rightleftharpoons H_3O^+ + OH^- \tag{3}$$

which has an equilibrium constant K_w of approximately 10^{-14}. In pure water, the law of mass action allows us to describe the effective concentration of the ions in water as:

$$1 \times 10^{-14} = \frac{[H_3O^+][OH^-]}{a_{H_2O}} \tag{4}$$

where a_{H_2O} is the activity of water; $[H_3O^+]$ and $[OH^-]$ are the molar concentration of hydronium and hydroxide ions in solution. The 1:1 ratio of Equation 3 leads to an effective concentration of 10^{-7}M for both ions in pure water.

$$[H_3O^+] = [OH^-] = 1 \times 10^{-7} M$$

Nevertheless, at pH 0, the introduction of 1M protons shifts the effective amount of hydroxide ions that can arise from the self-ionization of water.

$$1 \times 10^{-14}/[H_3O^+] = [OH^-] = 1 \times 10^{-14} M$$

Note that given the 1:1 ratio of Equation 3, this technically also means that proton ions from water are also produced at an effective concentration of 10^{-14}M during water self-ionization in acid (neglecting the protons introduced to make the solution acidic). As such, it takes an externally applied potential to ionize water molecules and form a standard concentration of protons and hydroxide ions:

$$\mathrm{H_2O + e^- \rightleftharpoons \frac{1}{2}H_2 + OH^-} \tag{5}$$

As shown in **Figure 1(a)**, the energy needed to form an atomic unit of H^+ and OH^- is related to the potential where H_2 gas can be formed from water ($-0.82V$ vs. SHE at pH 0). When an electrode potential of $-0.82V$ is applied, the chemical potential of the electrons on an electrode is high enough to meet the requirements for H–H bond formation via proton from *water*. The result is that one of the O–H bonds is broken, and a leftover OH^- from water ionization appears in acidic solution.

Note that in the process, the resulting OH^- can effectively be seen as a "negative" electrode floating in solution, with a potential of around $-0.82V$. Nearby protons can move to revert the hydroxide back to water. If every hydroxide produced from water splitting is subsequently protonated, then the pH of the solution should remain unchanged.

If protons are not being replenished, then the result is that our applied electrostatic work exposes every existing proton to the newly formed hydroxide ions. In an alkaline solution where the OH^- is at 1M, all remaining protons effectively feel a solution potential of $-0.82V$. This can be shown in **Figure 1(b)**, where the highly oxidizing environment of 1M OH^- solution leads to a 10^{-14}M effective concentration of protons. If we kept a working electrode

at 0V vs. SHE (the potential where the protons are in equilibrium with 1 bar of H_2 gas in acid), this solution is still biased such that it favors oxidizing the H_2 gas to introduce more protons into solution. It takes an externally applied potential of $-0.82V$ vs. SHE to counterbalance the solution potential from the exposed OH^- concentration. In **Figure 1(b)**, this is represented as $-0.82V$ vs. SHE.

Our applied potential embodies a buildup of charge on the electrode and results in an electric field that fights with the inherent electrostatic field from the OH^- concentration (or H^+ concentration) within the aqueous solvent. The RHE potential occurs when our electrode's applied potential overcomes the electrostatic field of the OH^- in the solvent, such that the protons in the solvent can start to move towards the electrocatalyst to form H* and H_2 gas.

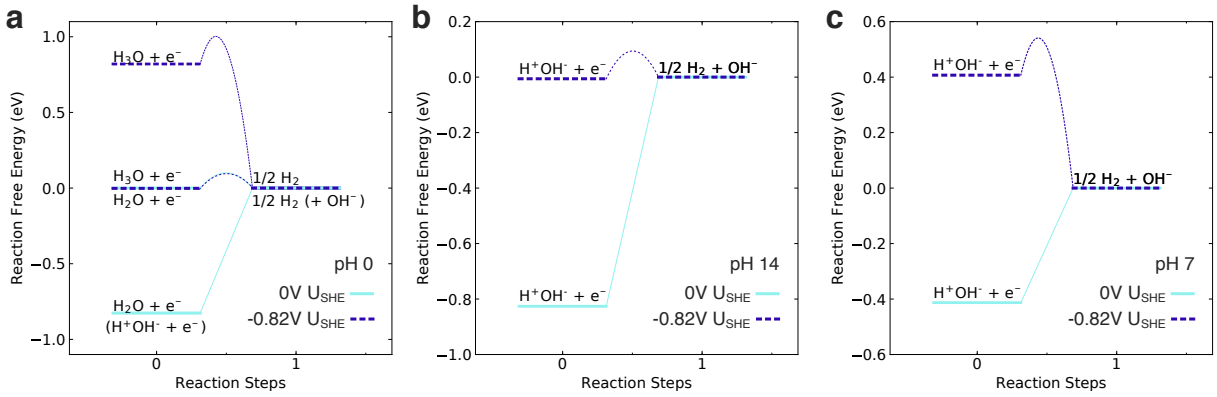

Figure 1: Free energy diagrams describing (a) hydronium and water reduction at a bulk pH of 0 (b, c) water reduction at pH 14 and 7, respectively. Each free energy diagram is referenced such that only the electrochemical potential of proton is adjusted for its solution concentration. At pH 0, proton and hydroxide ions are referenced to 1M and 10^{-14}M, respectively. At pH 14, the reverse concentration is applied. At pH 7, both ions are at 10^{-7}M. At 0V SHE, 1M proton state is referenced to H_2 gas and is also defined at 0. Applied potential $-eU$ is used to achieve water reduction at $-0.82V$ vs. SHE/RHE. Barriers are drawn for aesthetic purposes.

As noted in **Figure 1**, when the effective hydronium concentration is not at $1M$, the chemical potential of the proton will be adjusted via a concentration component:

$$\mu_{H^+(aq)} = \mu_{H_0^+(aq)} + 0.059 * log_{10}([H^+]) \tag{6}$$

This concentration term helps describe a specific phenomenon found in nature: that high concentration gradients migrate to low concentration gradients. Protons will spread out in solution like a gas. At pH 4, the proton free energy should be adjusted by a concentration energy term of $-0.059 * 4$ or $-0.236eV$ *relative to the proton state at 1M* and the H_2 state at 1 bar.

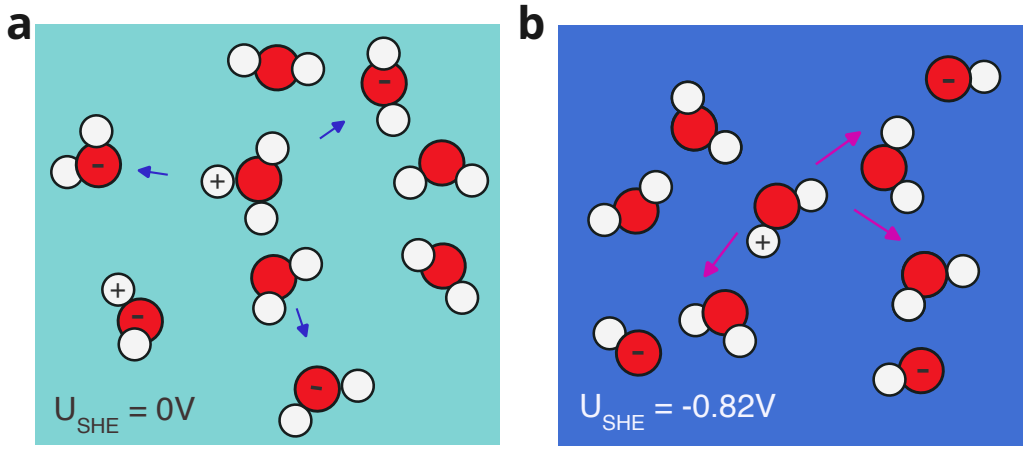

Figure 2: (a,b) In acidic solution (pH 0), protons from hydronium move between water molecules. The effective potential seen by the mobile proton is 0V vs. SHE. (f) In basic solution (pH 14), the remaining protons move between hydroxide ions. The effective potential seen by mobile protons is $-0.82V$ vs. SHE. Driven potentials steer protons in solution towards electrodes.

To keep track of the effective proton and hydroxide concentrations from water ionization, we can notate the state as H^+OH^-. This state also represents the transfer of protons between aqueous hydroxide ions (a constant transformation between hydroxides and water molecules) and is different from H_3O^+ that we originally start with in the acidic solution. In a solution without any electrodes and no external addition of hydronium or hydroxide ions, shuttling protons in acid and alkaline solutions can be described with the following equations:

$$H_3O^+ + H_2O \rightleftharpoons H_2O + H_3O^+ \tag{7}$$

$$OH^- + H_2O \rightleftharpoons H_2O + OH^- \tag{8}$$

Figure 2 shows a comparison of how protons are shuttled in acid and alkaline solutions as described by Equation 7 and Equation 8 respectively. At constant bulk pH of 0, any mobile proton from hydronium will observe a 0V vs. SHE potential when shuttling around the water network. This is contrasted in alkaline solutions, where the chemical potential of electron held by the solvated OH^- is exposed to all nearby cationic species as it constantly attempts to attract protons to reform back into water. In **Figure 2(b)**, a water molecule in highly alkaline solutions can collide with a nearby OH^- but ends up becoming an OH^- ion itself, as there are only a finite number of protons around in solution. *Note that simply shuttling protons about either solutions will not change the overall bulk pH (no protons are being consumed), unlike water splitting in acidic solution.*

Standard References of Species

For *each* water molecule that breaks apart, we are effectively making an *atomic unit* of both H^+ and OH^- which must be treated with a per-atom basis (following the principle of mass conservation). Hence one still needs to drive a large negative potential to start water splitting in acid as shown earlier in **Figure 1(a)**. This also means that whenever we are describing the adsorption of a surface intermediate, it should always be referenced to a consistent concentration value. If $\frac{1}{2}$ H_2 is used for H*, then it is always on level with 1M of aqueous protons.

As illustrated in **Figure 3**, consider a half cell where 1 bar of H_2 gas is oxidized on an idealized platinum-like electrode to introduce protons into a solution with less than 1M of protons. At the immediate atomistic surface of creating protons on Pt, the effective H* coverage should be close to $\theta = 1$. This is no different than what it would be under a highly acidic solution, and hence we can imagine that the protons coming off the *immediate* surface can be treated as though it is at 1M in concentration. However, because the bulk solution pH is less than 1M, the protons from the immediate surface quickly disperse away into the

system due to the concentration gradient. In the case of pH 7, the overall cell potential is $0.419V$ because we are exploiting the work from passing a high concentration of protons from the surface into a low concentration solution. The SHE-centric models would try and explain concentration migration with the added $-eU_{SHE}$ term as if it is the electrons that are the species with a concentration value. It is more consistent to take the electrode potential as an applied polarization (or more often the RHE scale) of the overall cell.

When referencing with pure water at pH 7, it is possible to also reference its ionic counterpart of 10^{-7}M H_3O^+ and OH^-. With an electrode potential of $-0.419V$, the H_3O^+ and OH^- state is lifted via the chemical potential of electrons to arrive at the 1M concentration, where water splitting occurs. We show in Supplemental Figure 1 that free energies of ions can still adjust for varying concentration. From the standard concentration, the chemical potential of OH^- as function of pH is adjusted as follows:

$$\mu_{OH^-(aq)} = \mu_{OH_0^-(aq)} - 0.059 * log_{10}([H^+]) \tag{9}$$

where $\mu_{OH_0^-(aq)}$ is the chemical potential of hydroxide ion at standard state (1M) and will be stabilized monotonically with lower pH, eventually realizing a -0.82eV reduction in energy at highly acidic conditions (pH 0).

The Quirks of Charge-Centric Models

To elucidate pH-dependent phenomena using the CHE model, recent literature proposed charge-centric electrode models where the chemical potential of the electron can be defined separately on the 'SHE potential' scale. This is used to rationalize how protonation kinetic barriers may shift according to the SHE potential of the electrode[33,43,44], whereas reaction energies between intermediate states remain invariant on the RHE scale. This leads to a confounding situation where the electrode has two kinds of electrons: one term which is

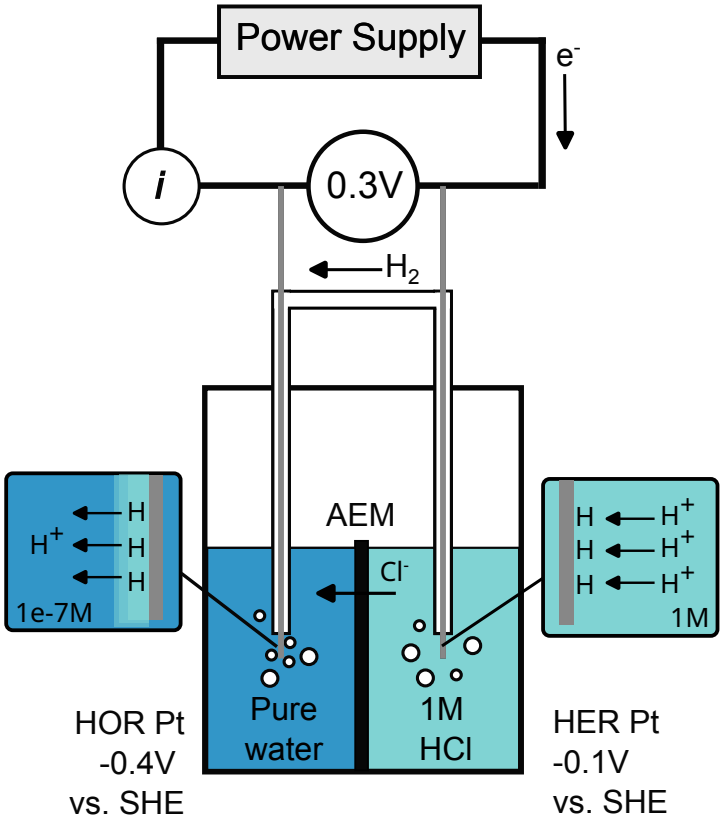

Figure 3: **Visualizing how concentration factors into the Nernst equation at pH 7.** A cell diagram depicting two platinized electrodes, where one electrode is immersed in 1M acid solution and generates H_2 gas. The gas is then brought to the other electrode performing hydrogen oxidation in pure water. The two half cells are connected with an anion exchange membrane. Atomistically, the hydrogen adsorbed on either electrode must have the same chemical activity; hence, hydrogens entering and leaving the active sites should yield the same effective concentration regardless of solution pH.

charged on the SHE scales from varying pH, and another term for the applied potential on the RHE scale.

Figure 4 illustrates how the charge-centric models make a distinction between electrons at the SHE potential and electrons at an "applied" RHE potential. Consider a two-electrode electrochemical cell setup in **Figure 4(a)**, where both electrodes are platinized 'reference' electrodes in a solution of pH 0. The potential between both electrode is 0V vs. SHE such that one electrode is running HER and the other is running HOR. Now if we start dumping KOH into the whole cell as shown in **Figure 4(b)**, it is clear that we remain at 0V vs. RHE because we have not applied any additional polarization between the two electrodes. In this scenario, the charge-centric models would suggest that reaction kinetics are altered by the SHE potential term ($-0.82V$ vs. SHE) whereas reaction energetics remain unchanged given the RHE scale. In our proposed model, we described that it is the introduction of high OH^- concentration that forces us to provide more electrostatic work to our electrodes to attract protons; the high SHE potential in alkaline conditions is for compensating the complex interplay between existing protons and the OH^- in solution. From these protons' perspective, no additional negative charge is being given to it. Hence, the RHE potential should be the predominant term in describing proton kinetics in alkaline solution.

The original CHE model maintains that reaction energies of intermediary steps are shifted linearly/Nernstian via electrochemical potential $\mu = \mu_0 + neU$, while the grand canonical model further extends the concept by adding plate capacitance free energetics based on the potential of zero charge of a given catalytic surface[19] relative to the SHE potential with which the electrode is at. This leads to a quadratic energy term relative to the potential of zero charge of the metal electrode.

The working assumptions of the plate capacitor model lead to certain issues. First, the potential of zero charge of most surfaces is notoriously hard to measure under reaction conditions[7,45,46]. In addition, the quadratic energetic formulation in grand canonical models

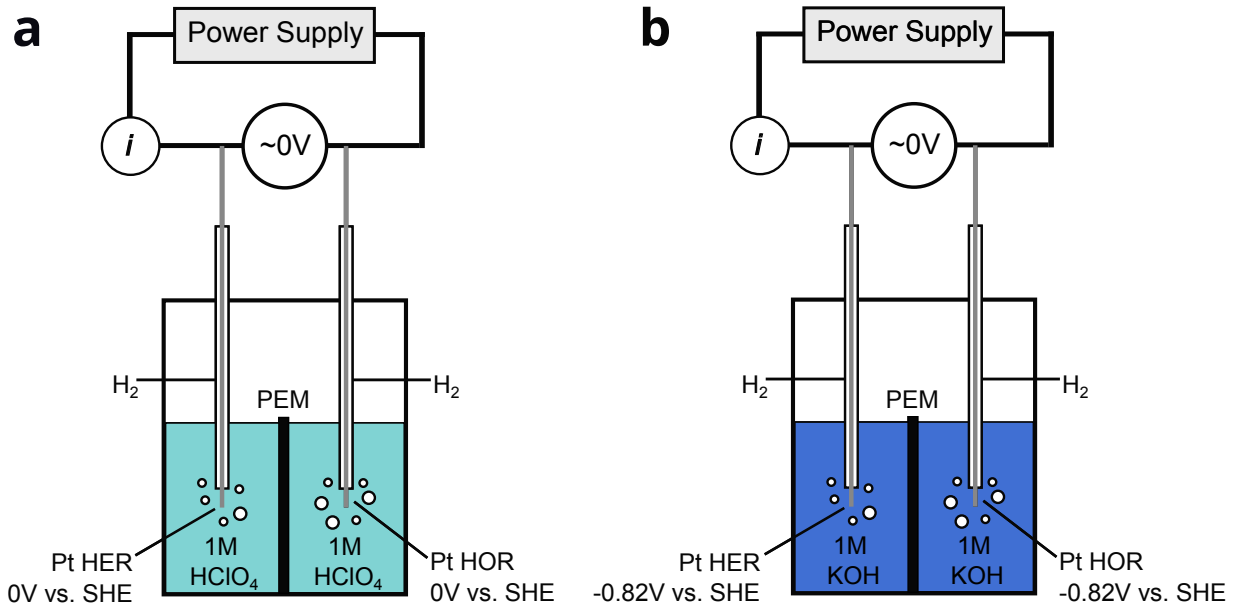

Figure 4: **Visualizing how "reference" potential changes with pH.** (a) Cell diagram with both electrodes are platinized electrodes and immersed in 1M $HClO_4$ solution. (b) Cell diagram with both electrodes immersed in 1M KOH solution.

leads to a peculiar problem as illustrated in **Figure 5**. It is entirely possible to set up an electrochemical cell where *both* electrodes are 'negatively' charged with respect to their potential of zero charge. This suggests that there are excess negative surface charges on both electrodes, leading to an influence on the electron chemical potential in driving electrochemical reactions. Yet, we know from the Nernst equation that the total reaction driving force of the electrochemical cell should simply be the chemical potential difference between the reactant and product *excluding* the chemical potential of the electrons and protons. For example, water splitting can be written as two half-cell reactions:

$$4H^+ + 4e^- \rightleftharpoons 2H_2 \tag{10}$$

$$2H_2O \rightleftharpoons O_2 + 4H^+ + 4e^- \tag{11}$$

But we can cancel out the protons and electrons to obtain the overall reaction as:

$$2H_2O \rightleftharpoons 2H_2 + O_2 \tag{12}$$

This can lead to a conservation of energy violation where the quadratic capacitor-like energetics from excess surface charges do not ever fall out neatly. Capacitor-like energetics in grand canonical models are also often used to explain additional changes to adsorption free energetics of intermediate states but not gas phase energetics[29,30,33,47–50]. The assumed countercharge used in grand canonical DFT to maintain a constant potential might not reflect the actual countercharge(s) in a full electrochemical cell. Likewise grand canonical methods typically assume static water layers to describe the electrochemical double layering near the catalytic surface. Currently, it remains speculative whether electrosorbed species based on the quadratic energetic formulation should be treated similar to chemisorbed species for Faradaic redox reactions[51].

Acidic HER vs. Alkaline HER

Table 1 shows the typical OH* binding energy referenced to H_2O - $\frac{1}{2}$ H_2 compared with the intrinsic adsorption energy of aqueous OH^- on common late-transition metal surfaces. Ag(111) is observed to slightly bind free OH^-[52,53]; while Au(111) poorly adsorbs free OH^-. While Pt(111) binds OH^- somewhat weakly, Pt(211) is vulnerable to OH^- adsorption, which may corroborate with experimental evidence of adsorbed OH^- found even at potentials where under deposition hydrogen is observed[54,55]. This model also suggests that hydroxides do adsorb on Cu surfaces, which various experiments have observed[32,56–60]. We note that the adsorption energetics above reflect the nature of oxidizing environment under 1M OH^- concentration; a similar environment would be oxidation via 0.2bar of O_2 in open air, where the chemical potential of O_2 also does not change upon reaction with an exposed oxophilic surface. In a closed thermodynamic system, adsorption driving force may change if the

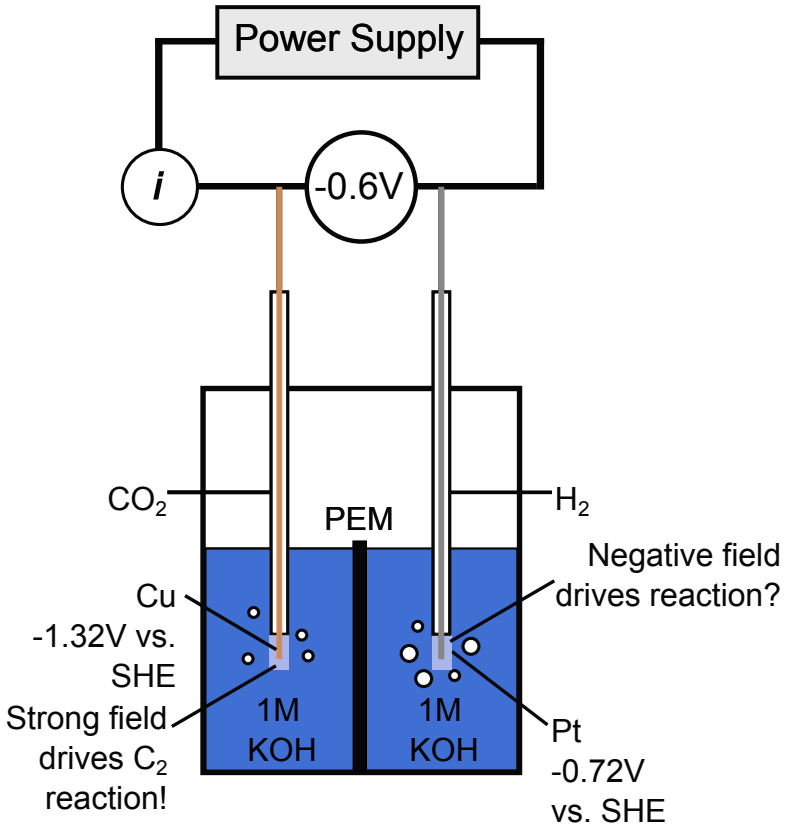

Figure 5: **Electrostatic charging conundrum between cathodes and anodes**. One electrode is performing CO_2 reduction with copper (Cu) electrode, while the other electrode performs hydrogen oxidation reaction with Pt electrode. With known potential of zero charge values for both metals, it is possible for both electrode surfaces to be treated capacitively as negatively charged.

concentration of ions near the surface fluctuates.

Table 1: **Free energy of H*, OH*, and OH^-*.** Adsorbed H* is referenced to $\frac{1}{2}$ H_2, OH* is referenced to H_2O and $\frac{1}{2}$ H_2, and OH^- is referenced to standard concentration at 1M. Even late transition metals are considered candidates for OH^- adsorption. Only vibrational free energy corrections are included. No solvation corrections applied. $\Delta G_{(M-OH^-H^+)}$ is the effective proton adsorption energy on an already adsorbed OH^- on the particular metal surface. In bold are metal-hydroxide sites that have nearly ideal proton adsorption energies for shuttling protons to the platinum surface.

M	ΔG_{H*}	ΔG_{OH*}	ΔG_{OH^-*}	$\Delta G_{(M-OH^-H^+)}$
Au(111)	0.48	1.51	0.68	-1.50
Ag(111)	0.48	0.83	0.01	-0.83
Pt(111)	-0.19	1.07	0.24	-1.07
Pt(211)	-0.35	0.43	-0.40	-0.43
Cu(111)	0.17	0.44	-0.38	-0.43
Cu(100)	0.20	0.25	-0.58	-0.24
Rh(111)	-0.18	0.52	-0.31	-0.51
Ni(111)	**-0.25**	**0.20**	**-0.63**	**-0.19**
Ru(0001)	**-0.38**	**0.05**	**-0.77**	**-0.04**
Co(0001)	**-0.37**	**-0.08**	**-0.915**	**0.09**

Figure 6 proposes a scheme of how alkaline HER differs from acidic HER. In highly alkaline solutions, applied potentials will drive an electrochemical potential gradient for protons produced by ionized water to pass along other OH^- molecules before arriving at the electrode surface. The sluggish reductive performance of water splitting comes from proton activity fluctuations along the alkaline shuttling pathway. With the ability to reference OH^-*, we are able to articulate whether a surface will adsorb hydroxide as an electrochemical species and how it influences reduction reactions. As mentioned earlier in **Figure 3**, protons (or surface hydrogens) immediately at the surface of Pt should have an activity similar to protons

in 1M concentration regardless of pH. So, from the perspective of any surface hydrogen, it should always leave the surface as "1M of concentration". As mentioned earlier, the 10^{-14}M concentration of proton in alkaline solution describes the eventual dilution of existing protons over an abundance of solvated OH^-; for any proton moving in solution via an external field, we expect that the proton is effectively 1M in concentration as water splitting must produce ion species of a consistent concentration.

Even under applied potentials, there is a possibility that surface hydrogens are constantly under electrostatic interaction with nearby hydroxide ions. Hence, the proton activity becomes a balancing act at the interface[61]. As shown in **Figure 6(a)**, we can imagine that any underpotential deposited H* on the surface of Pt(111) can always be readily attacked by OH^- to form water. But given that protons in solution must shuttle through a chain of OH^- to get to the surface, the interaction between OH^- and surface hydrogen will incur a cost of bringing protons from solution to the surface. We conjecture that there exists a pseudo-hydronium layer (which we will call H_{dh}) that denotes the activity of mobile protons near the Pt surface given interaction from any nearby OH^- interacting with H*. The cost of building this hydronium layer is assumed to be the H* binding energy of the metal itself. **Figure 6(b)** shows a free energy diagram that depicts the need for a proton layer H_{dh} created as OH^- interacts with surface H*.

Figure 6(c,d) illustrates the migration of protons through a metal decorated layer in alkaline conditions. When Pt(111) is decorated with a reasonably oxophilic metal like nickel, any nearby OH^- can be stabilized by the decorated metal islands without the need for H_{dh} layer. While the adsorbed OH^- on nickel can still be 'reduced' into water with incoming protons, the reaction energy to reduce it to water is also the effective proton binding energy with respect to the immediate Pt surface (which we will call M-OH^-H^+). At water-splitting potentials, the applied polarization on the electrode will further ionize the freshly formed water around the nickel sites back into proton and OH^-. In the last column of Table 1, we

show that Ru(0001) and Co(0001) have M-OH^-H^+ binding energetics that are close to ideal. This means their M-OH^- state is relatively like the H_2O gas state. The reaction force that produces water in metal hydroxides should be the same driving force for bringing protons towards the Pt surface. Hence, any water molecule formed on metal hydroxides immediately act as proton sources for Pt to use and make H_2 gas under water reduction conditions.

We can use the energetics of Table 1 to build a microkinetic model where protons from water splitting are transferred from the bulk to the Pt(111) surface, which is shown in **Figure 7**. In this model the H* binding energy of Pt(111) is still reference to 1M H^+ or $\frac{1}{2}$ H_2 just like the CHE model. The main deviation from HER in acidic conditions is the interaction of nearby OH^- [62]. This model differs from past literature that claims that the pH effect between alkaline HER and acidic HER comes from varying kinetic barriers between H_3O and H_2O as proton sources[33,44], rather than fluctuations in proton activity.

Anions on Cathodes

A common misconception is that a negatively charged ion does not adsorb on a 'negatively charged' electrode (cathode). Several examples of observed free anion adsorption at the cathode such as the following: chloride or chlorate interference in alkaline oxygen reduction on gold (Au) and silver (Ag)[64–66]; acidic and alkaline nitrate reduction[4,67,68]; zincate reduction into zinc[69,70]; and anion-mediated HER[71]. Coulombic repulsion arises when there are notable charge imbalances at the electrode interfaces. Applying a cathodic potential (whether it is $-0.8V$ vs. RHE or $0.7V$ vs. SHE) only suggests electrochemical potential differences between electrodes in the whole cell. It does not necessarily mean that that electrode builds up a substantial 'negative charge' as counter charges will work to maintain electroneutrality conditions near electrode interfaces (on both cathodes and anodes). With reactions happening on the surface, excess charges on the electrode are also expected to leave as Faradaic current. Protons will take up excess charge and proceed to evolve hydrogen; protons may

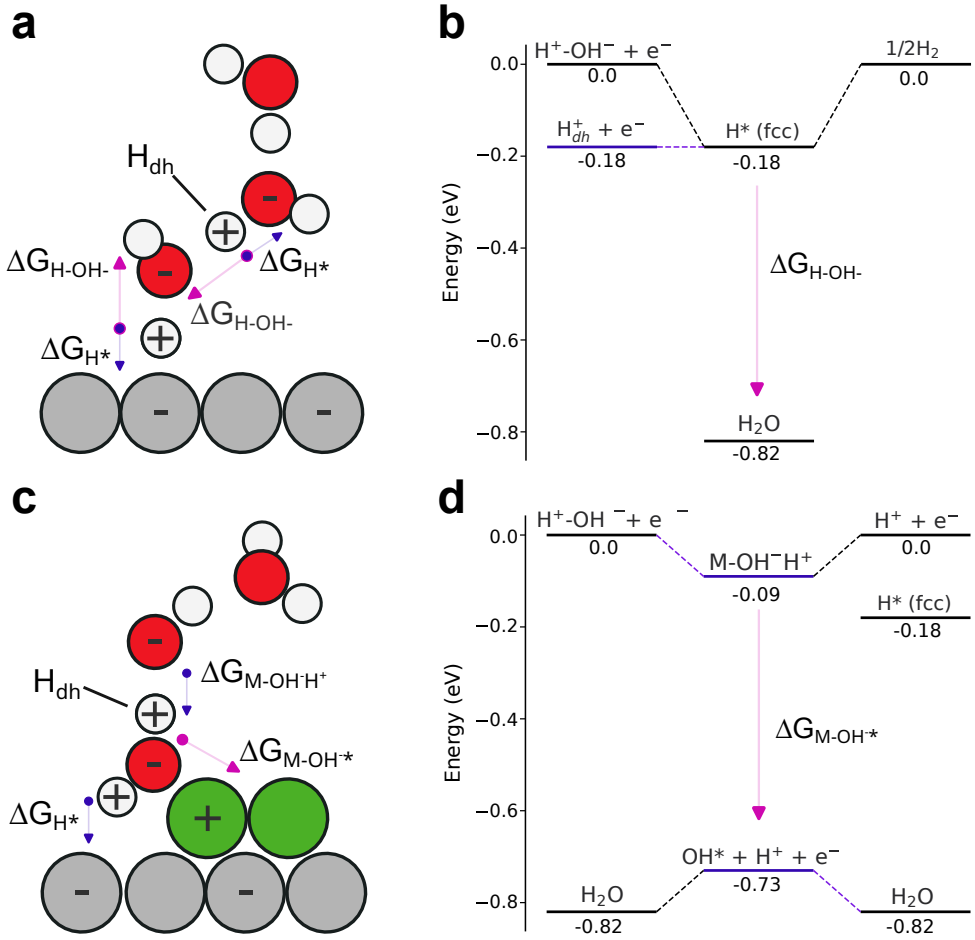

Figure 6: **The effects of metal-hydroxides on alkaline HER** (a, c) Close to the Pt surface (in grey atoms), the effective activity of the protons is modulated by surrounding hydroxide ions. (a) shuttling protons across free-standing hydroxides requires the formation of a pseudo-hydronium transition state complex. The energetics of the complex relative to the free-moving proton can be estimated based on the hydrogen binding energy of the surface. (b) the presence of metal-hydroxides facilitates proton shuttling; Ni atoms on Pt surface are colored in green. (b,d) Free energy diagram of passing a proton through a metal hydroxide-decorated Pt surface. Metals that strongly adsorbed hydroxide will enable a smoother transfer of protons through its interface towards the Pt surface. By default, protons can also bring OH^- close to the surface at the expense of available H* for HER.

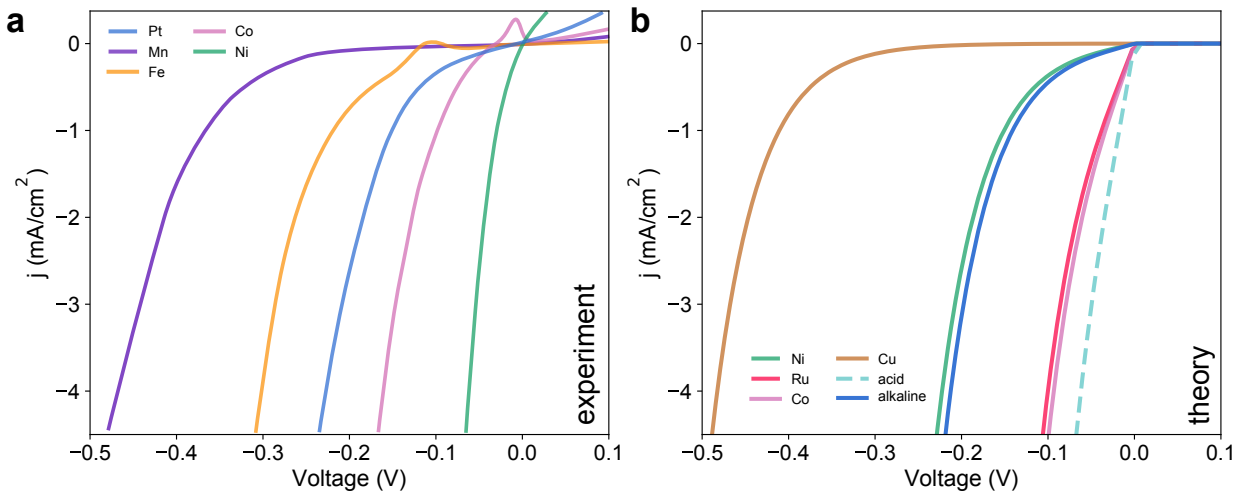

Figure 7: **Trends in the exchange currents observed with hydrogen evolution in alkaline solution on Pt(111) and metal-decorated Pt surface.** (a) Experimental polarization curve of hydrogen evolution reaction in alkaline conditions on Pt(111), reproduced from Strmcnik et al.[63]. (b) Simulated polarization curve of hydrogen evolution reaction in alkaline conditions with given the scheme of OH^- energy vs. Pt(111).

even force the exchange of anions that adsorb on the surface[72].

Literature often uses the CHE model to justify that OH* cannot exist on late transition metal surfaces under reducing conditions, as the binding energetics of OH* is too weak and would quickly reduce off the surface as water with little to no applied potential[31]. 1M OH^- differs from OH* because it already has an electrostatic charge associated with it; and in the *absence* of proton motion due to electrostatic fields, a free roaming OH^- will still be attracted to any nearby positively charged element. We assume transition metal electrodes are not exempt from hydroxide attack. The addition of protons will adjust the chemical potential of OH^- as to account for the co-interaction between the two species.

Modeling Alkaline CO_2R on (100) Surfaces of Au and Ag

With a standard OH^- reference, the CIME model can help clarify the 2-electron pathway for CO_2 reduction to formate and CO in alkaline condition. The two pathways can be written

as:

$$CO_2 + H_2O + 2e^- \rightleftharpoons CO + 2OH^- \tag{13}$$

$$CO_2 + H_2O + 2e^- \rightleftharpoons HCOO^- + OH^- \tag{14}$$

When the typical CHE model is applied, we can only realize intermediate states based on proton-electron transfer steps. Thus, we are forced to go through either COOH* or HCOO* from CO_2(g) + H^+ + e^-. For Ag and Au, the prohibitive COOH* binding energy suggests an alternative way to reach CO(g). Note that in the CHE model, the COOH* state is also referenced to H_2O to form CO upon a second proton-electron transfer. Because the energetics of COOH* are prohibitively high on the coinage metals, there must be a way to rationalize the binding energy disparity between COOH* and HCOO*.

Past literature have suggested CO_2^- as a possible intermediate in 2-electron pathway for CO_2 reduction on Au and Ag[73,74]. The adsorption energetics CO_2^- on coinage metals remains elusive within DFT. This is because CO_2^- is an excited state relative to CO_2 gas and bends due to local electrostatic forces applied to it[75]. Also note that when CO_2^- is formed at the cathode, it should be treated as an *anion*; thus, in order to maintain electroneutrality, we technically need to add back a proton or some cation into the half-cell reaction equation. We can quantify the energy of CO_2^- + H^+ relative to CO_2(g) + H^+ + e^- (included in Figure 8). Sterically, CO_2^- is most like either formate ($HCOO^-$) or oxalate ($C_2O_4^{2-}$). Both can be derived from their acidic counterpart via observed pKa values:

$$HCOOH \leftrightharpoons HCOO^- + H^+, pKa = 3.75 \tag{15}$$

$$HOOCCOOH \leftrightharpoons OOCCOO^{2-} + 2H^+, pKa = 4.2 \tag{16}$$

Based on thermochemical data, the redox potential of CO_2 to oxalic acid is $-0.43V$ vs. SHE. Hence, the chemical potential difference between gaseous CO_2 and $\frac{1}{2}$ oxalic acid is roughly

0.43eV. After adjusting by $0.059eV * pKa$, the chemical potential of $\frac{1}{2}$ oxalate is around 0.55eV above CO_2(g). This is a reasonable estimate of CO_2^- that corroborates with past literature (~0.6eV)[76,77] Compton et al.[78]. Solvated CO_2^- should be thermoneutral with oxalate ions, such that there is little to no driving force towards forming oxalate with solvated CO_2^-. Another study finds that the pKa between COOH radical and CO_2^- + H^+ is only 3.4[79], which is similar to formic acid. As an *anion*, we will conjecture that CO_2^- can interact with the surface as a physiosorbed state, with a $0.55eV$ formation barrier from solvated CO_2.

Under alkaline conditions, the formation of CO should form OH^- instead of H_2O. With the new electrode model, we claim the existence of an adsorbed $COOH^{-}$* intermediate as referenced to CO and OH^-. The $COOH^{-}$* state is effectively the COOH* state but shifted downward by $0.82eV$ because of the ionization cost between H_2O and H^+ + OH^-. From solvated CO_2^-, the formation of $COOH^{-}$* can be described as a coupled proton-electron transfer step which is energetically surmountable for even Au(100) and Ag(100) provided an electron is transferred along with a proton. Using solvated OH^- as a reference, the pathway as shown in **Figure 8** can be realized.

Given the arguments above, we can model the CO pathway as a multi-electron step where one proton and two electrons are transferred to form $COOH^{-}$*. The formation of $COOH^{-}$* now can be referenced to CO + OH^- instead of CO + H_2O(g). The energy difference between COOH* and $COOH^{-}$* is 0.82eV because the oxygen in COOH* is technically referenced to H_2O, whereas $COOH^{-}$* is now referenced to H^+OH^-. Using H^+OH^- as the reference signifies that the OH^- is free-floating and any cation can represent the positively charged counterion. In the *absence* of alkali-metal cations[80], the predominant cation in solution would be protons, which can be easily reduced away under CO_2 reducing potentials. When pH decreases from 14 to 0, $COOH^{-}$* will become less stabilized because the effective energy of H^+OH^- approaches the energy of H_2O as shown in Supplemental Figure 1 or **Equation 9**, reverting back to the COOH* state from the CHE model.

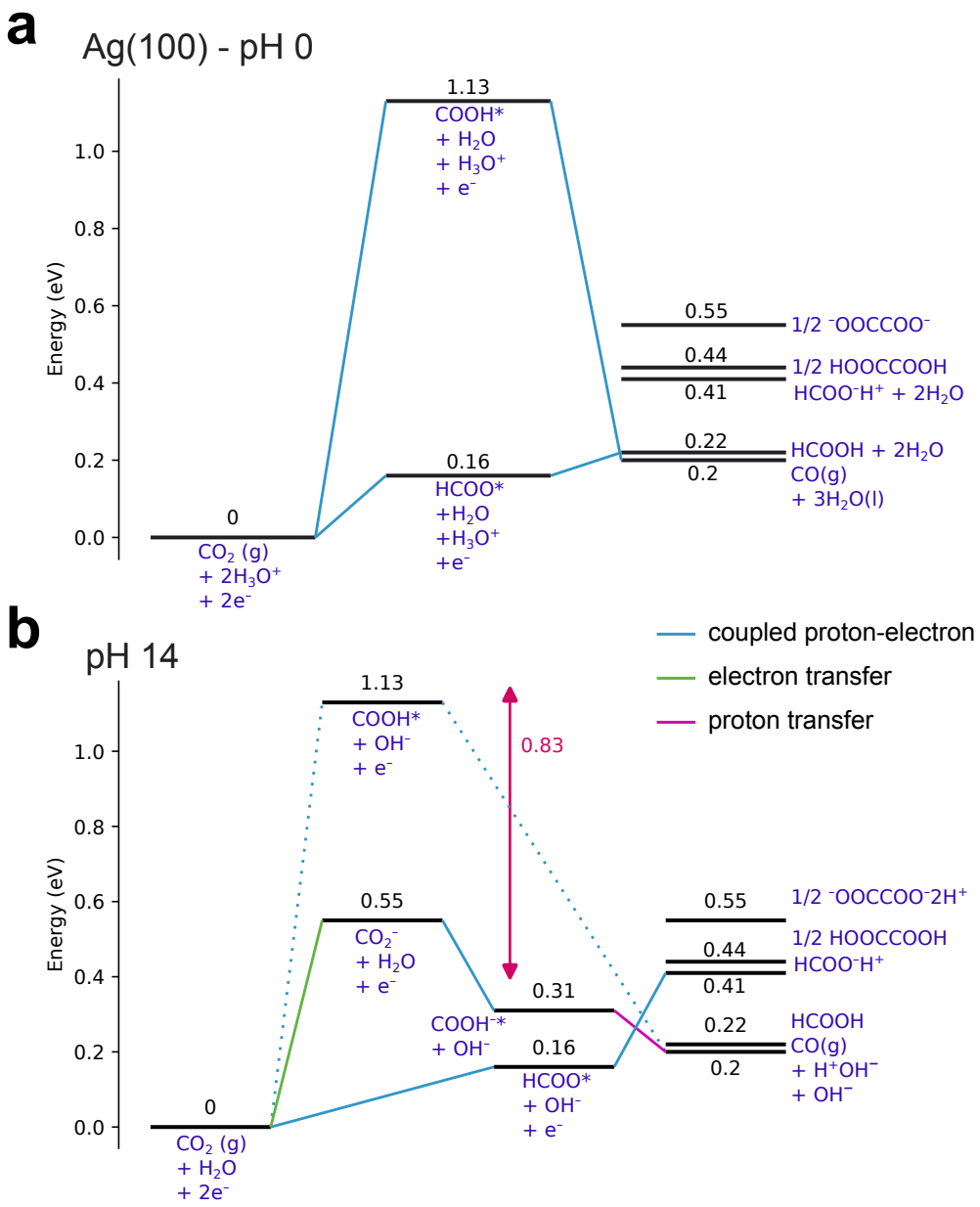

Figure 8: Free energy diagram of CO_2R that shows the first two steps to form $HCOO^-$ and CO. Using the acidic CHE reference of the CO_2 and $\frac{1}{2}\mu_{H_2}$ technically captures the energetic of COOH*. To form CO, we provide a second proton to form H_2O and CO; thus, the COOH* intermediate state is also referenced to CO + H_2O. However, one needs to reference this energy state to CO + OH^- in order to visualize an equivalent state in alkaline conditions. Note that all gas references between CO_2, CO and formate are still maintained such that the redox potentials between the gases are consistent with experimentally reported values. No additional solvation corrections are applied. A full diagram with barriers used in CATMAP is provided as Supplemental Figure 2 and 3. An equivalent pathway can be constructed from HCO_3^- or CO_3^{2-} as references. For clarity's sake, we also provide a separate diagram to portray these references in the Supplemental Information.

For the formate pathway, we still assume that the formation of HCOO* follows a CHE-style reference, using $\frac{1}{2}H_2$ from ionized water. The limiting step of $HCOO^-$ formation is the desorption of the intermediate. Hence the five reactions steps of CO_2 reduction on all three metals under alkaline conditions are modeled as:

1. $CO_2 + e^- \rightleftharpoons CO_2^-*$
2. $CO_2^- + H_2O + e^- \rightleftharpoons COOH^- * + OH^-(aq)$
3. $COOH^-* \rightleftharpoons CO(g) + OH^-(aq)$
4. $CO_2 + H_2O + e^- \rightleftharpoons HCOO * + OH^-(aq)$
5. $HCOO * + e^- \rightleftharpoons HCOO^-(aq)$

This allows us to see that the "binding" energy differences between HCOO* and $COOH^-$* are in fact quite close on all three metals. Cu is notable for its ability to bind $COOH^-$* favorably unlike Ag and Au relative to CO(g) and OH^- in aqueous solution. This means any CO* on the Cu surface *can* form bonds with OH^-(aq)* and become a surface intermediate, much like bicarbonate formation between CO_2(g) and OH^- in solution. We hypothesize that this can be a factor as to why Cu can reduce CO with ease compared to Ag and Au. We will show how this affects mechanisms in CO_2R and COR on Cu(100) in a follow-up work.

A naive microkinetic model can be made for Ag(100) using the energetics shown in Figure 8 alongside certain assumptions on reaction kinetics and transport kinetics. For protonation kinetics, we conjecture that the barrier to form an O-H bond for COOH-* is still smaller than the formation of the C-H bond for HCOO*, by setting the barriers at equilibrium for reaction step (2) and step (4) to be 0.6eV and 0.8eV, respectively. We assume similar prefactors ($\frac{k_B T}{h}$) for all reaction steps[84]. We stress to the readers that the protonation barriers chosen are entirely arbitrary and are simply inspired by trends observed from barrier calculations done by Patel et al.[85] and Shi et al.[86]. We note that most protonation barrier calculations done thus far in previous DFT works (even from the authors) have all required a parallel-plate capacitor model in order to capture their energetics, which the validity of this condition is

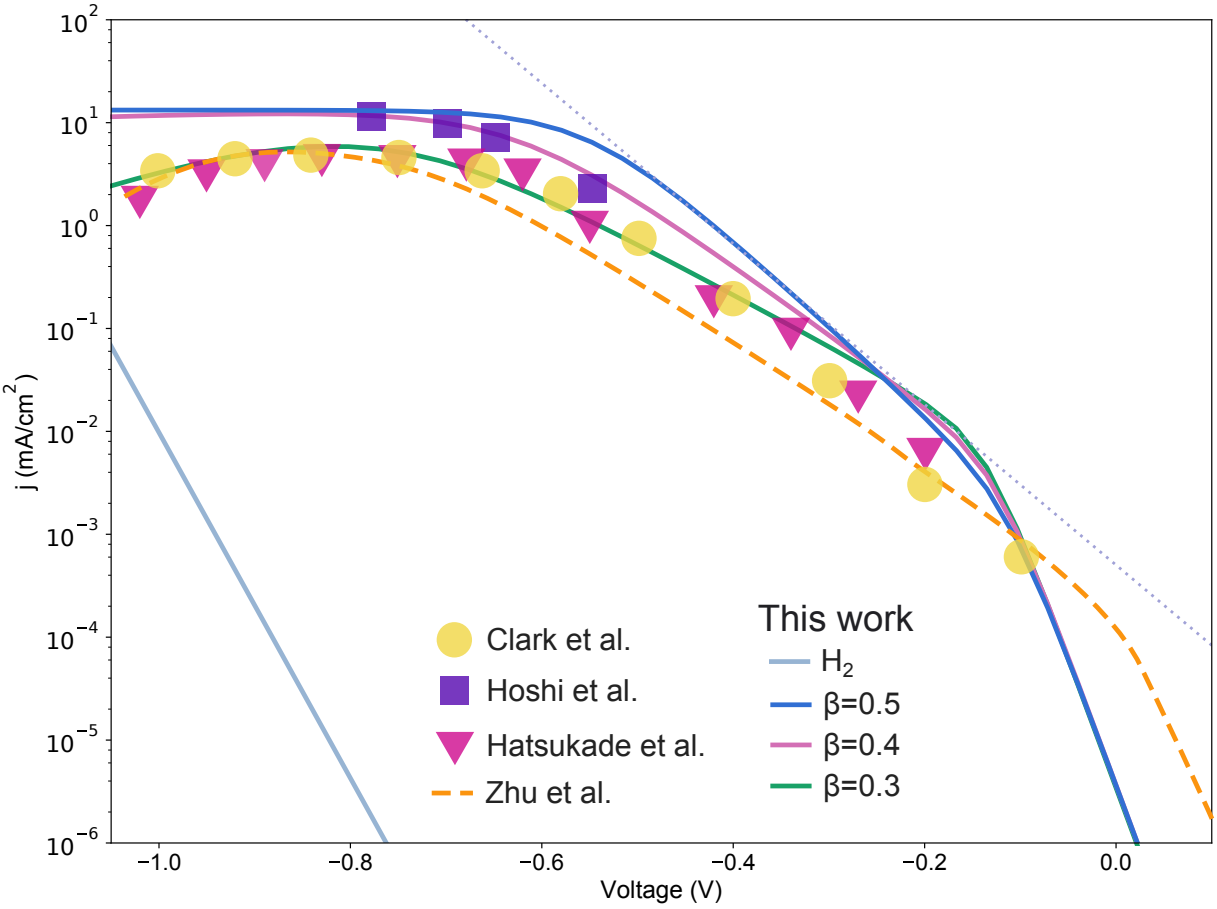

Figure 9: **Tafel plot of two-electron CO_2 reduction on Ag.** We compare our microkinetic model, varying charge transfer coefficient for step 1, with one provided by Zhu et al.[81], with the inclusion of experimental points by Clark et al.[82], Hatsukade et al.[73], and Hoshi et al.[83].

still speculative when driving substantial Faradaic currents. Likewise, any barriers computed via grand canonical models have similar assumptions and drawbacks. For transport kinetics, we introduce a simple diffusion layer where the effective activity of the 'gaseous' reactants (OH^-, and H^+) is modulated through 'electrochemical' barriers where the charge transfer coefficient β is set to 0. This diffusion layer is set between the surface sites that perform the catalysis and the bulk gaseous environment that is provided to CATMAP as the reactant input, so it technically represents the local reaction environment of the catalyst. In this transport model, we assume there is little to no difference in the effective electrochemical activity of reactants in the bulk environment and the diffusion layer close to the surface. Turnover frequencies from CATMAP are estimated as current densities following established assumptions regarding surface site density and number of electrons transferred per reactant-to-product pathway[87].

Overall, we show that the mechanism proposed above allows us to reach the onset potentials for CO formation on Ag(100) observed from experimental results as shown in Figure 9. We provide microkinetic results for Au(100) in the Supplemental Figure 4 and 5[49,74,81,88]. Figure 9 also shows the polarization curve for Ag using RHE scale and is thus relevant to both pH 7 and pH 14. Furthermore, we also can simulate the minor formation of formate on Ag(100) as detected by experiments done by Hatsukade et al.[73]. Due to limited scope, we will present similar ion-based microkinetic models going from CO_2 or CO to ethylene and methane on Cu(100) in a follow-up work in the near future.

Implications

The electrode model in this work challenges the necessity of using solvation effects and capacitive field effects to rationalize thermodynamic steps in alkaline environments. Thermodynamic steps like COOH* can now be referenced to OH^-(aq). Hence, just like the original CHE model was suitable for describing potential-limiting steps in ORR and HER in acidic

conditions, the CIME model provides a deterministic way of describing the potential-limiting steps in alkaline conditions. While the binding energies of adsorbates relative to their references should not really change, the energetics of steps involving protons and electrons will still change with potential.

Like the original CHE model, the CIME model does not attempt to describe kinetics. Within the framework of DFT, methods for determining kinetic barriers remain unclear without assumptions of a parallel plate capacitor. When simulating metal slabs, any explicit water layer(s) will automatically impose an electrostatic field based on its orientation. The addition of a proton or cation also ends up transferring its charge to the Fermi level of the metal slab, consequentially charging the whole system[35,89]. These phenomena may become problematic when working with reaction free energetics because slab systems are typically modeled as a half-cell rather than a whole cell.

Nonetheless, a notable feature of the CIME model is that we can still apply CHE-like $\frac{1}{2}\mu_{H_2}$ as our hydrogen source. At water splitting potentials, the proton generated from ionizing water should be no different from a proton in acid. In fact, the CHE model fortuitously works in highly acidic solutions *because* the protons come from strong acids, where the anions are chosen to have little to no interactions with protons nor the surface. At all pH levels, a proton can come from any electrolyte with an ionizable proton to donate. A proton donor can be a hydronium, water, or even a buffer species like bicarbonate[71]. The pH level is maintained when protons from the anode can replenish protons that are reduced into H_2 gas, even when using a buffer as a stockpile of protons. Nevertheless, as soon as $-0.41V$ vs. RHE is reached at pH 7, water splitting conditions may alter mechanistic pathways for certain reactions as we will discuss in a future work.

The CIME model shows that OH^- adsorbs electrostatically to the majority of late-transition metal surfaces, even under cathodically driven potentials. This is because at potentials beyond water-splitting, any additional bias will begin depriving $OH^{-}*$ of protons. This can

lead to a possibility of surface poisoning or corrosion via OH^{-}*[9,90–92], which the mechanisms are also currently being investigated on Cu.

Conclusions and Outlook

The current work shows that it is possible to model electrochemical reactions in alkaline environment by considering the ionized form of proton donors. Water reduction requires two molecules of water to form H_2 and leaves two molecules of OH^- in solution. Water has an inherent self-ionization constant ($K_w = 10^{14}$) at room temperature, and one can derive the chemical potential of $1M$ OH^- from it. If we take 1 bar H_2 gas as our reference for 1M protons, then the energetic state of hydroxide ions at standard concentration is *always* $0.828eV$ higher in energy than water. This constant difference of *intrinsic* chemical potential/ activity between water and the $1M$ OH^- is what enables water reduction at -0.41V vs. RHE at pH 7. When intermediates are referenced with $1M$ OH^-, we can describe new intermediate states that are relevant specifically under water splitting conditions.

In the CIME model, the SHE potential is rather described as the interaction between mobile protons with existing anions in solution; externally driven potentials can be described with the RHE potential or other redox couples. Anions serve as protonic resistors in solution; they impede the flow of protons when we apply a polarization to our electrochemical cell. Differing anions will affect the protonic driving force to perform any electrochemical reactions. The difference in proton behavior under alkaline environments exemplifies the importance of understanding the energetic interplay between ionic species in electrochemical microenvironments.

Nevertheless, when modeling electrochemical reactions, there remain two contending schools of thought regarding the role of electrons (and how to model with them via DFT). The original CHE model suggests an a posteriori linear shifting of $-eU$ performed outside of DFT calculations to adjust the free energies of thermodynamic steps along an overall half reaction.

In contrast, the grand canonical models attempt to determine the electronic energetics by applying bias directly in the DFT cell with an absolute potential scale. Biases within DFT cells may contribute an additional quadratic correction, enabling capacitor-like qualities of the electrochemical double layer within DFT. The main benefit of the linear shift is that it follows the electrochemical potential μ from the Nernst equation and can be applied a posteriori; however, a capacitor-like model remains a necessity for determining kinetic barriers when modeling metal-water interfaces atomistically at the present time. The CIME model does not provide a definitive answer to how electrochemical kinetics should be modeled. It remains to be seen if electrochemical barriers on electrode surfaces can be computed efficiently in periodic DFT, with or without well-defined double layer structures.

Methods

Reaction energetics were calculated with density functional theory (DFT) with a periodic plane-wave implementation and ultrasoft pseudopotentials using the QUANTUM ESPRESSO code, interfaced with the Atomistic Simulation Environment (ASE). We applied the BEEF-vdW functional, which provides a reasonable description of van der Waals forces while maintaining an accurate prediction of chemisorption energies. Plane-wave and density cutoffs were 500 and 5000 eV, respectively, with a Fermi-level smearing width of 0.1 eV. psLib ultrasoft pseudopotentials were chosen. The adsorption energies on (100) surfaces of face-centered cubic transition metals were evaluated using four-layer (3×3) supercells with the bottom two layers constrained and a vacuum layer of 20 Å, and $[4 \times 4 \times 1]$ Monkhorst-Pack k-point grids.

Microkinetic modeling. Mean-field microkinetic models were simulated with the CATMAP software package. The CatMAP software package used in this work can be accessed and downloaded through https://github.com/SUNCAT-Center/catmap. We provide the complete microkinetic model for HER on decorated Pt(111) and Ag(100) for CO_2R from this

work as supplementary information.

Acknowledgement

This research was supported by the U.S. Department of Energy, Office of Science, Office of Basic Energy Sciences, Chemical Sciences, Geosciences, and Biosciences Division, Catalysis Science Program to the SUNCAT Center for Interface Science and Catalysis. The material is also inspired by work performed by the Liquid Sunlight Alliance, which is supported by the U.S. Department of Energy, Office of Science, Office of Basic Energy Sciences, Fuels from Sunlight Hub under Award Number DE-SC0021266. We acknowledge the use of the computer time allocation at the National Energy Research Scientific Computing Center, a DOE Office of Science User Facility supported by the Office of Science of the U.S. Department of Energy under Contract No. DE-AC02-05CH11231.

Supplemental Info

DFT tabulated gas and reaction energies regarding HER and CO_2RR. Tabulated energy corrections values used are provided. Additional data from the microkinetic model for HER and CO_2 shown in this work is provided. Full microkinetic models shown in this work are provided.

References

(1) Shih, A. J. et al. Water electrolysis. *Nat Rev Methods Primers* **2022**, *2*, 1–19.

(2) Shinagawa, T.; Takanabe, K. Electrocatalytic Hydrogen Evolution under Densely Buffered Neutral pH Conditions. *J. Phys. Chem. C* **2015**, *119*, 20453–20458.

(3) Hausmann, J. N.; Schlögl, R.; Menezes, P. W.; Driess, M. Is direct seawater splitting economically meaningful? *Energy Environ. Sci.* **2021**, *14*, 3679–3685.

(4) Liu, J.-X.; Richards, D.; Singh, N.; Goldsmith, B. R. Activity and Selectivity Trends in Electrocatalytic Nitrate Reduction on Transition Metals. *ACS Catal.* **2019**, *9*, 7052–7064.

(5) Anderson, A. Insights into electrocatalysis. *Physical chemistry chemical physics : PCCP* **2011**, *14*, 1330–8.

(6) Schmickler, W. Double layer theory. *J Solid State Electrochem* **2020**, *24*, 2175–2176.

(7) Rebollar, L.; Intikhab, S.; Oliveira, N. J.; Yan, Y.; Xu, B.; McCrum, I. T.; Snyder, J. D.; Tang, M. H. "Beyond Adsorption" Descriptors in Hydrogen Electrocatalysis. *ACS Catal.* **2020**, *10*, 14747–14762.

(8) Melander, M. M. Frozen or dynamic? — An atomistic simulation perspective on the timescales of electrochemical reactions. *Electrochimica Acta* **2023**, *446*, 142095.

(9) Marcus, P.; Maurice, V.; Strehblow, H. H. Localized corrosion (pitting): A model of passivity breakdown including the role of the oxide layer nanostructure. *Corrosion Science* **2008**, *50*, 2698–2704.

(10) Weitzner, S. E.; Dabo, I. First Principles Simulations of Electrified Interfaces in Electrochemistry; John Wiley & Sons, Ltd, 2021; pp 439–472.

(11) Peljo, P.; Girault, H. H. Electrochemical potential window of battery electrolytes: the HOMO–LUMO misconception. *Energy Environ. Sci.* **2018**, *11*, 2306–2309.

(12) Debye, Peter; Hückel, Erich Zur Theorie der Elektrolyte I; Physikalische Zeitschrift: Berlin, Heidelberg, 1923; pp 185–206, 305–325.

(13) Guggenheim, E. A. The Conceptions of Electrical Potential Difference between Two Phases and the Individual Activities of Ions. *J. Phys. Chem.* **1929**, *33*, 842–849.

(14) The quantum mechanics of electrolysis. *Proc. R. Soc. Lond. A* **1931**, *134*, 137–154.

(15) Santos, E.; Schmickler, W. Models of Electron Transfer at Different Electrode Materials. *Chem. Rev.* **2022**, *122*, 10581–10598.

(16) Trasatti, S. The absolute electrode potential: an explanatory note (Recommendations 1986). *Pure and Applied Chemistry* **1986**, *58*, 955–966.

(17) Benedikt, U.; Schneider, W. B.; Auer, A. A. Modelling electrified interfaces in quantum chemistry: constant charge vs. constant potential. *Phys. Chem. Chem. Phys.* **2013**, *15*, 2712–2724.

(18) Abidi, N.; Lim, K. R. G.; Seh, Z. W.; Steinmann, S. N. Atomistic modeling of electrocatalysis: Are we there yet? *WIREs Computational Molecular Science* **2021**, *11*, e1499.

(19) Taylor, C. D.; Wasileski, S. A.; Filhol, J.-S.; Neurock, M. First principles reaction modeling of the electrochemical interface: Consideration and calculation of a tunable surface potential from atomic and electronic structure. *Phys. Rev. B* **2006**, *73*, 165402.

(20) Warburton, R. E.; Soudackov, A. V.; Hammes-Schiffer, S. Theoretical Modeling of Electrochemical Proton-Coupled Electron Transfer. *Chem. Rev.* **2022**, *122*, 10599–10650.

(21) Ge, A.; Videla, P. E.; Lee, G. L.; Rudshteyn, B.; Song, J.; Kubiak, C. P.; Batista, V. S.; Lian, T. Interfacial Structure and Electric Field Probed by *in Situ* Electrochemical Vibrational Stark Effect Spectroscopy and Computational Modeling. *J. Phys. Chem. C* **2017**, *121*, 18674–18682.

(22) Groß, A. Grand-canonical approaches to understand structures and processes at electrochemical interfaces from an atomistic perspective. *Current Opinion in Electrochemistry* **2021**, *27*, 100684.

(23) Doblhoff-Dier, K.; Koper, M. T. M. Electric double layer of Pt(111): Known unknowns and unknown knowns. *Current Opinion in Electrochemistry* **2023**, *39*, 101258.

(24) Nørskov, J. K.; Rossmeisl, J.; Logadottir, A.; Lindqvist, L.; Kitchin, J. R.; Bligaard, T.; Jónsson, H. Origin of the Overpotential for Oxygen Reduction at a Fuel-Cell Cathode. *J. Phys. Chem. B* **2004**, *108*, 17886–17892.

(25) Ping, Y.; Nielsen, R. J.; Goddard, W. A. I. The Reaction Mechanism with Free Energy Barriers at Constant Potentials for the Oxygen Evolution Reaction at the IrO2 (110) Surface. *J. Am. Chem. Soc.* **2017**, *139*, 149–155.

(26) Gao, G.; Wang, L.-W. A potential and pH inclusive microkinetic model for hydrogen reactions on Pt surface. *Chem Catalysis* **2021**, *1*, 1331–1345.

(27) Huang, J.; Chen, S.; Eikerling, M. Grand-Canonical Model of Electrochemical Double Layers from a Hybrid Density–Potential Functional. *J. Chem. Theory Comput.* **2021**, *17*, 2417–2430.

(28) Baricuatro, J. H.; Kwon, S.; Kim, Y.-G.; Cummins, K. D.; Naserifar, S.; Goddard, W. A. I. Operando Electrochemical Spectroscopy for CO on Cu(100) at pH 1 to 13: Validation of Grand Canonical Potential Predictions. *ACS Catal.* **2021**, *11*, 3173–3181.

(29) Zhang, Z.; Wei, Z.; Sautet, P.; Alexandrova, A. N. Hydrogen-Induced Restructuring of a Cu(100) Electrode in Electroreduction Conditions. *J. Am. Chem. Soc.* **2022**, *144*, 19284–19293.

(30) Chen, L. D.; Urushihara, M.; Chan, K.; Nørskov, J. K. Electric Field Effects in Electrochemical CO2 Reduction. *ACS Catal.* **2016**, *6*, 7133–7139.

(31) Kamat, G. A.; Zamora Zeledón, J. A.; Gunasooriya, G. T. K. K.; Dull, S. M.; Perryman, J. T.; Nørskov, J. K.; Stevens, M. B.; Jaramillo, T. F. Acid anion electrolyte

effects on platinum for oxygen and hydrogen electrocatalysis. *Commun Chem* **2022**, *5*, 1–10.

(32) Dinh, C.-T.; Burdyny, T.; Kibria, M. G.; Seifitokaldani, A.; Gabardo, C. M.; Arquer, F. P. G. d.; Kiani, A.; Edwards, J. P.; Luna, P. D.; Bushuyev, O. S.; Zou, C.; Quintero-Bermudez, R.; Pang, Y.; Sinton, D.; Sargent, E. H. CO2 electroreduction to ethylene via hydroxide-mediated copper catalysis at an abrupt interface. *Science* **2018**, *360*, 783–787.

(33) Peng, H.; Tang, M.; Liu, X.; Schlexer Lamoureux, P.; Bajdich, M.; Abild-Pedersen, F. The Role of Atomic Carbon in Directing Electrochemical CO(2) Reduction to Multicarbon Products. **2019**,

(34) Gauthier, J. A.; Dickens, C. F.; Heenen, H. H.; Vijay, S.; Ringe, S.; Chan, K. Unified Approach to Implicit and Explicit Solvent Simulations of Electrochemical Reaction Energetics. *J. Chem. Theory Comput.* **2019**, *15*, 6895–6906.

(35) Chan, K.; Nørskov, J. K. Electrochemical Barriers Made Simple. *J. Phys. Chem. Lett.* **2015**, *6*, 2663–2668.

(36) Luan, D.; Xiao, J. Adaptive Electric Fields Embedded Electrochemical Barrier Calculations. *J. Phys. Chem. Lett.* **2023**, *14*, 685–693.

(37) Ludwig, T.; Gauthier, J. A.; Brown, K. S.; Ringe, S.; Nørskov, J. K.; Chan, K. Solvent–Adsorbate Interactions and Adsorbate-Specific Solvent Structure in Carbon Dioxide Reduction on a Stepped Cu Surface. *The Journal of Physical Chemistry C* **2019**, *123*, 5999–6009.

(38) Rossmeisl, J.; Chan, K.; Ahmed, R.; Tripković, V.; Björketun, M. E. pH in atomic scale simulations of electrochemical interfaces. *Phys. Chem. Chem. Phys.* **2013**, *15*, 10321–10325.

(39) Pasumarthi, V.; Yu, H.; Akhade, S. A.; Abild-Pedersen, F.; Varley, J. B.; Bajdich, M. A Comparative Study of Electrical Double Layer Effects for CO Reduction Reaction Kinetics. *J. Phys. Chem. C* **2023**, *127*, 16850–16860.

(40) Tanaka, Y. Water dissociation in ion-exchange membrane electrodialysis. *Journal of Membrane Science* **2002**, *203*, 227–244.

(41) Stuve, E. M. Ionization of water in interfacial electric fields: An electrochemical view. *Chemical Physics Letters* **2012**, *519-520*, 1–17.

(42) Saitta, A. M.; Saija, F.; Giaquinta, P. V. *Ab Initio* Molecular Dynamics Study of Dissociation of Water under an Electric Field. *Phys. Rev. Lett.* **2012**, *108*, 207801.

(43) Liu, X.; Schlexer, P.; Xiao, J.; Ji, Y.; Wang, L.; Sandberg, R. B.; Tang, M.; Brown, K. S.; Peng, H.; Ringe, S.; Hahn, C.; Jaramillo, T. F.; Nørskov, J. K.; Chan, K. pH effects on the electrochemical reduction of CO(2) towards C2 products on stepped copper. *Nature Communications* **2019**, *10*.

(44) Lamoureux, P. S.; Singh, A. R.; Chan, K. pH Effects on Hydrogen Evolution and Oxidation over Pt(111): Insights from First-Principles. *ACS Catal.* **2019**, *9*, 6194–6201.

(45) Bockris, J. O., Conway, B. E., Yeager, E., Eds. Comprehensive Treatise of Electrochemistry; Springer US: Boston, MA, 1980.

(46) Xu, P.; von Rueden, A. D.; Schimmenti, R.; Mavrikakis, M.; Suntivich, J. Optical method for quantifying the potential of zero charge at the platinum–water electrochemical interface. *Nat. Mater.* **2023**, *22*, 503–510.

(47) Gao, G.; Wang, L.-W. Substantial potential effects on single-atom catalysts for the oxygen evolution reaction simulated via a fixed-potential method. *Journal of Catalysis* **2020**, *391*, 530–538.

(48) Alsunni, Y. A.; Alherz, A. W.; Musgrave, C. B. Electrocatalytic Reduction of CO2 to CO over Ag(110) and Cu(211) Modeled by Grand-Canonical Density Functional Theory. *J. Phys. Chem. C* **2021**, *125*, 23773–23783.

(49) Ringe, S.; Morales-Guio, C. G.; Chen, L. D.; Fields, M.; Jaramillo, T. F.; Hahn, C.; Chan, K. Double layer charging driven carbon dioxide adsorption limits the rate of electrochemical carbon dioxide reduction on Gold. *Nature Communications* **2020**, *11*, 33.

(50) Huang, J.; Li, M.; Eslamibidgoli, M. J.; Eikerling, M.; Groß, A. Cation Overcrowding Effect on the Oxygen Evolution Reaction. *JACS Au* **2021**, *1*, 1752–1765.

(51) Hörmann, N. G.; Marzari, N.; Reuter, K. Electrosorption at metal surfaces from first principles. *npj Comput Mater* **2020**, *6*, 1–10.

(52) Horswell, S. L.; Pinheiro, A. L. N.; Savinova, E. R.; Danckwerts, M.; Pettinger, B.; Zei, M.-S.; Ertl, G. A Comparative Study of Hydroxide Adsorption on the (111), (110), and (100) Faces of Silver with Cyclic Voltammetry, Ex Situ Electron Diffraction, and In Situ Second Harmonic Generation. *Langmuir* **2004**, *20*, 10970–10981.

(53) Jovic, B. M.; Jovic, V. D.; Stafford, G. R. Cyclic voltammetry on Ag(111) and Ag(100) faces in sodium hydroxide solutions. *Electrochemistry Communications* **1999**, *1*, 247–251.

(54) Janik, M. J.; McCrum, I. T.; Koper, M. T. On the presence of surface bound hydroxyl species on polycrystalline Pt electrodes in the "hydrogen potential region" (0–0.4 V-RHE). *Journal of Catalysis* **2018**, *367*, 332–337.

(55) McCrum, I. T.; Koper, M. T. M. The role of adsorbed hydroxide in hydrogen evolution reaction kinetics on modified platinum. *Nat Energy* **2020**, *5*, 891–899.

(56) Kunze, J.; Maurice, V.; Klein, L. H.; Strehblow, H.-H.; Marcus, P. In Situ Scanning Tunneling Microscopy Study of the Anodic Oxidation of Cu(111) in 0.1 M NaOH. *J. Phys. Chem. B* **2001**, *105*, 4263–4269.

(57) Kunze, J.; Maurice, V.; Klein, L. H.; Strehblow, H.-H.; Marcus, P. In situ STM study of the duplex passive films formed on Cu(111) and Cu(001) in 0.1 M NaOH. *Corrosion Science* **2004**, *46*, 245–264.

(58) Auer, A.; Ding, X.; Bandarenka, A. S.; Kunze-Liebhäuser, J. The Potential of Zero Charge and the Electrochemical Interface Structure of Cu(111) in Alkaline Solutions. *J. Phys. Chem. C* **2021**, *125*, 5020–5028.

(59) Yamamoto, S.; Andersson, K.; Bluhm, H.; Ketteler, G.; Starr, D. E.; Schiros, T.; Ogasawara, H.; Pettersson, L. G. M.; Salmeron, M.; Nilsson, A. Hydroxyl-Induced Wetting of Metals by Water at Near-Ambient Conditions. *J. Phys. Chem. C* **2007**, *111*, 7848–7850.

(60) Iijima, G.; Inomata, T.; Yamaguchi, H.; Ito, M.; Masuda, H. Role of a Hydroxide Layer on Cu Electrodes in Electrochemical CO2 Reduction. *ACS Catal.* **2019**, *9*, 6305–6319.

(61) Chen, M.; Zheng, L.; Santra, B.; Ko, H.-Y.; DiStasio Jr, R. A.; Klein, M. L.; Car, R.; Wu, X. Hydroxide diffuses slower than hydronium in water because its solvated structure inhibits correlated proton transfer. *Nature Chem* **2018**, *10*, 413–419.

(62) Sheng, W.; Zhuang, Z.; Gao, M.; Zheng, J.; Chen, J. G.; Yan, Y. Correlating hydrogen oxidation and evolution activity on platinum at different pH with measured hydrogen binding energy. *Nat Commun* **2015**, *6*, 5848.

(63) Strmcnik, D.; Lopes, P. P.; Genorio, B.; Stamenkovic, V. R.; Markovic, N. M. Design principles for hydrogen evolution reaction catalyst materials. *Nano Energy* **2016**, *29*, 29–36.

(64) Blizanac, B. B.; Ross, P. N.; Marković, N. M. Oxygen Reduction on Silver Low-Index Single-Crystal Surfaces in Alkaline Solution: Rotating Ring Disk $_{Ag(\ h\ \ kl\ )}$ Studies. *J. Phys. Chem. B* **2006**, *110*, 4735–4741.

(65) Blizanac, B. B.; Lucas, C. A.; Gallagher, M. E.; Arenz, M.; Ross, P. N.; Marković, N. M. Anion Adsorption, CO Oxidation, and Oxygen Reduction Reaction on a Au(100) Surface: The pH Effect. *J. Phys. Chem. B* **2004**, *108*, 625–634.

(66) Blizanac, B. B.; Ross, P. N.; Markovic, N. M. Oxygen electroreduction on Ag(111): The pH effect. *Electrochimica Acta* **2007**, *52*, 2264–2271.

(67) Liu, M. J.; Guo, J.; Blair, S. J.; Nielander, A. C.; Jaramillo, T. F.; Tarpeh, W. A. Electrodialysis and Nitrate Reduction to Synthesize and Recover Ammonia from Wastewaters. *Meet. Abstr.* **2020**, *MA2020-02*, 1546.

(68) Bae, S.-E.; Stewart, K. L.; Gewirth, A. A. Nitrate Adsorption and Reduction on Cu(100) in Acidic Solution. *J. Am. Chem. Soc.* **2007**, *129*, 10171–10180.

(69) Igarashi, K.; Aramata, A.; Taguchi, S. Underpotential deposition of zinc ions and specific adsorption of hydroxyl species at Pt(111) in alkaline solutions. *Electrochimica Acta* **2001**, *46*, 1773–1781.

(70) Dirkse, T. P. The Behavior of the Zinc Electrode in Alkaline Solutions: V . Supersaturated Zincate Solutions. *J. Electrochem. Soc.* **1981**, *128*, 1412–1415.

(71) Marcandalli, G.; Boterman, K.; Koper, M. T. M. Understanding hydrogen evolution reaction in bicarbonate buffer. *Journal of Catalysis* **2022**, *405*, 346–354.

(72) Lucky, C.; Schreier, M. Mind the Interface: The Role of Adsorption in Electrocatalysis. *ACS Nano* **2024**, *18*, 6008–6015.

(73) Hatsukade, T.; Kuhl, K. P.; Cave, E. R.; Abram, D. N.; Jaramillo, T. F. Insights into

the electrocatalytic reduction of CO2 on metallic silver surfaces. *Phys. Chem. Chem. Phys.* **2014**, *16*, 13814–13819.

(74) Chen, Y.; Li, C. W.; Kanan, M. W. Aqueous CO2 Reduction at Very Low Overpotential on Oxide-Derived Au Nanoparticles. *J. Am. Chem. Soc.* **2012**, *134*, 19969–19972.

(75) Gauthier, J. A.; Fields, M.; Bajdich, M.; Chen, L. D.; Sandberg, R. B.; Chan, K.; Nørskov, J. K. Facile Electron Transfer to CO2 during Adsorption at the Metal|Solution Interface. *J. Phys. Chem. C* **2019**, *123*, 29278–29283.

(76) Calaza, F.; Stiehler, C.; Fujimori, Y.; Sterrer, M.; Beeg, S.; Ruiz-Oses, M.; Nilius, N.; Heyde, M.; Parviainen, T.; Honkala, K.; Häkkinen, H.; Freund, H.-J. Carbon Dioxide Activation and Reaction Induced by Electron Transfer at an Oxide–Metal Interface. *Angewandte Chemie International Edition* **2015**, *54*, 12484–12487.

(77) Freund, H.-J.; Roberts, M. Surface chemistry of carbon dioxide. *Surface Science Reports* **1996**, *25*, 225–273.

(78) Compton, R. N.; Reinhardt, P. W.; Cooper, C. D. Collisional ionization of Na, K, and Cs by CO2, COS, and CS2: Molecular electron affinities. *The Journal of Chemical Physics* **1975**, *63*, 3821–3827.

(79) Janik, I.; Tripathi, G. N. R. The nature of the CO2− radical anion in water. *The Journal of Chemical Physics* **2016**, *144*, 154307.

(80) Monteiro, M. C. O.; Dattila, F.; Hagedoorn, B.; García-Muelas, R.; López, N.; Koper, M. T. M. Absence of CO2 electroreduction on copper, gold and silver electrodes without metal cations in solution. *Nat Catal* **2021**, *4*, 654–662.

(81) Zhu, X.; Huang, J.; Eikerling, M. Electrochemical CO2 Reduction at Silver from a Local Perspective. *ACS Catal.* **2021**, *11*, 14521–14532.

(82) Clark, E. L.; Ringe, S.; Tang, M.; Walton, A.; Hahn, C.; Jaramillo, T. F.; Chan, K.; Bell, A. T. Influence of Atomic Surface Structure on the Activity of Ag for the Electrochemical Reduction of CO2 to CO. *ACS Catal.* **2019**, *9*, 4006–4014.

(83) Hoshi, N.; Kato, M.; Hori, Y. Electrochemical reduction of CO2 on single crystal electrodes of silver Ag(111), Ag(100) and Ag(110). *Journal of Electroanalytical Chemistry* **1997**, *440*, 283–286.

(84) Bard, A. J.; Faulkner, L. R. Electrochemical methods: fundamentals and applications. 2nd ed.; Wiley: New York, 2001.

(85) Patel, A. M.; Vijay, S.; Kastlunger, G.; Nørskov, J. K.; Chan, K. Generalizable Trends in Electrochemical Protonation Barriers. *J. Phys. Chem. Lett.* **2021**, *12*, 5193–5200.

(86) Shi, C.; Chan, K.; Yoo, J. S.; Nørskov, J. K. Barriers of Electrochemical CO2 Reduction on Transition Metals. *Org. Process Res. Dev.* **2016**, *20*, 1424–1430.

(87) Hansen, H. A.; Viswanathan, V.; Nørskov, J. K. Unifying Kinetic and Thermodynamic Analysis of 2 e– and 4 e– Reduction of Oxygen on Metal Surfaces. *J. Phys. Chem. C* **2014**, *118*, 6706–6718.

(88) Singh, M. R.; Goodpaster, J. D.; Weber, A. Z.; Head-Gordon, M.; Bell, A. T. Mechanistic insights into electrochemical reduction of CO2 over Ag using density functional theory and transport models. *PNAS* **2017**, *114*, E8812–E8821.

(89) Chen, L. D.; Bajdich, M.; Martirez, J. M. P.; Krauter, C. M.; Gauthier, J. A.; Carter, E. A.; Luntz, A. C.; Chan, K.; Nørskov, J. K. Understanding the apparent fractional charge of protons in the aqueous electrochemical double layer. *Nat Commun* **2018**, *9*, 3202.

(90) Flemming, H.-C., Murthy, P. S., Venkatesan, R., Cooksey, K., Eds. Marine and In-

dustrial Biofouling; Springer Series on Biofilms; Springer Berlin Heidelberg: Berlin, Heidelberg, 2009; Vol. 4.

(91) Kolotyrkin, J. M. Effects of Anions on the Dissolution Kinetics of Metals. *J. Electrochem. Soc.* **1961**, *108*, 209.

(92) Sarker, Hori Pada; Goswami, Anshuman; Tang, Michael T; Abild-Pedersen, Frank Mechanistic Insights into Cu Cathodic Corrosion: Unveiling the role of Alkaline HER. *in submission*

TOC entry